Direct observation of an optically induced charge density wave transition in 1*T*-$TaSe_2$

Shuaishuai Sun,[1] Linlin Wei,[1] Zhongwen Li,[1] Gaolong Cao,[1] Y. Liu,[2] W. J. Lu,[2] Y. P. Sun,[3,4] Huanfang Tian,[1] Huaixin Yang,[1,*] and Jianqi Li[1,5,†]

[1]*Beijing National Laboratory for Condensed Matter Physics, Institute of Physics, Chinese Academy of Sciences, Beijing 100190, China*
[2]*Key Laboratory of Materials Physics, Institute of Solid State Physics, Chinese Academy of Sciences, Hefei 230031, China*
[3]*High Magnetic Laboratory, Chinese Academy of Sciences, Hefei 230031, China*
[4]*Collaborative Innovation Center of Advanced Microstructures, Nanjing University, Nanjing 210093, China*
[5]*Collaborative Innovation Center of Quantum Matter, Beijing 100190, China*

(Received 1 June 2015; revised manuscript received 10 November 2015; published 2 December 2015)

Four-dimensional ultrafast transmission electron microscopy measurements reveal a rich variety of structural dynamic phenomena at a phase transition in the charge density wave (CDW) of 1*T*-$TaSe_2$. Under photoexcitation, remarkable changes in both the CDW intensity and orientation are clearly observed, associated with the transformation from a commensurate (C) phase into an incommensurate (IC) phase in a time scale of picoseconds. Moreover, the transient states reveal a notable "structural isosbestic point" at a wave vector of q_{iso} where the C and IC phases yield their diffracting efficiencies in equal ratio. This observation reveals that the crystal planes parallel to q_{iso} adopt a common dynamic feature in the CDW phases throughout whole nonequilibrium transition. The second-order characteristics observed in this nonequilibrium phase transition have also been analyzed based on time-resolved structural data.

DOI: 10.1103/PhysRevB.92.224303 PACS number(s): 71.45.Lr, 64.70.Rh, 68.37.Lp, 78.47.J−

The charge density wave (CDW), with inherent modulation of electron density and associated periodic lattice distortion, is a typical cooperative phenomenon arising from strong coupling between electron and phonon in a quasi-one-dimensional (or two-dimensional) metallic material, and the CDW state often competes and/or coexists with other ordered states, such as superconductivity [1,2]. In recent decades, intense theoretical and experimental efforts have been devoted to understanding the origin of the CDW [3,4]. Most recently, studies employing ultrafast spectroscopy have revealed a variety of notable dynamic features in CDW compounds, including coherently driven collective modes [5] and photoinduced phase transitions [6–8]. Moreover, ultrafast electron diffraction (UED) [9–12], ultrafast x-ray diffraction [11–14], and four-dimensional ultrafast transmission electron microscopy (4D-UTEM) [15–20] have been demonstrated to be effective in revealing ultrafast structural changes at time resolutions better than one picosecond. In the transition-metal dichalcogenides, experimental observations reveal that photoinduced dynamics often involves multiple transient steps in different time scales [21–23]. The periodic lattice generally undergoes an initial fast decay in a few hundred femtoseconds following optically induced redistribution of electron density, and then a rapid electron-phonon energy transfer is followed by a recovery of the CDW when the excess energy is redistributed by thermalization. Recent ultrafast studies have also demonstrated the presence of remarkable transient hidden states in 1*T*-TaS_2 [24], providing more insights for understanding the nature of the phenomena cooperating in these CDW materials. Furthermore, nonequilibrium CDW phase transition triggered by photoexcitation often shows different features in comparison with those observed in thermal equilibrium transformation [22]. In this paper, we report on a study of the CDW phase transition in 1*T*-$TaSe_2$ between a commensurate phase (C phase, $q_C = 0.225a^* + 0.07b^*$) and an incommensurate phase (IC phase, $q_{IC} = 0.278a^*$) employing 4D-UTEM. Theoretical analysis of the topology of the Fermi surface suggests that CDW in the IC phase of 1*T*-$TaSe_2$ can be connected by the modulation wave vector as predicted by the Peierls model [3,25]; however, the nature of the C phase and CDW transitions is still under debate [26–29]. Our measurements reveal notably fast rotation of CDW vectors, and moreover a notable "structural isosbestic point" has been identified for this nonequilibrium CDW transient. Certain fundamental features for the structural transition and the threshold effects of photoexcitation for the CDW modulations have also been discussed for this layered system.

1*T*-$TaSe_2$ has a layered crystalline structure, consisting of planes of hexagonally arranged tantalum (Ta) atoms sandwiched by two selenium (Se) layers coordinating the central Ta atom in an octahedral arrangement. The three-atom-thick Se-Ta-Se layers are weakly bound via a Van der Waals interaction along the *c*-axis direction [see Fig. 1(a)]. The atomic structure associated with the CDW modulations in our sample was first examined using high-resolution scanning transmission electron microscopy (STEM), as shown in Fig. 1(b), in which the superstructure associated with the commensurate modulations is well identified and illustrated schematically in an inset. It is clear that each supercell contains the six nearest and six next-nearest Ta neighbors of the central Ta atom, shifting inward and forming a 13-atom star-of-David cluster [30–32]. In the literature, it is well demonstrated that CDW transitions in 1*T*-$TaSe_2$ change both resistivity and structural properties [1,3]. The CDW transition from IC phase to C phase occurs at 470 K, yielding a visible angular rotation (∼13°) of the CDW wave vector, as shown in Fig. 1(c).

Single-crystalline samples used in the present study have been well characterized, as reported in Ref. [1]. In our UTEM experiments, the 1*T*-$TaSe_2$ single crystals were mounted on well-aligned multiwalled carbon nanotube (MWCNT)

*hxyang@aphy.iphy.ac.cn
†ljq@aphy.iphy.ac.cn

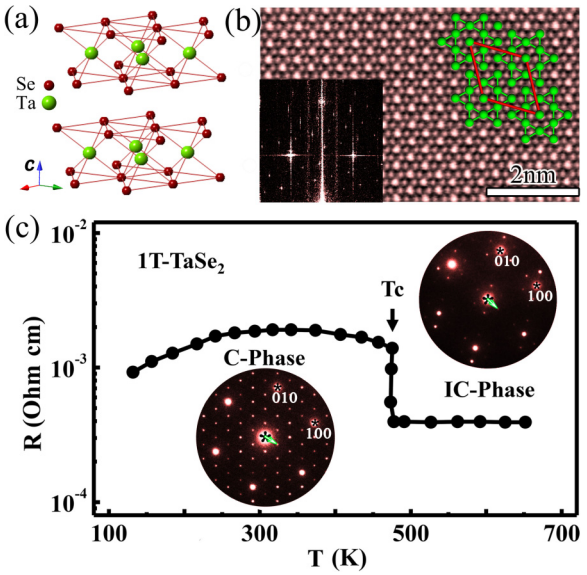

FIG. 1. (Color online) (a) Structural model of $1T$-$TaSe_2$ with a layered structure. (b) High-resolution STEM image of CDW modulation in $1T$-$TaSe_2$; the inset at the top right corner is a schematic illustration of the q_C superstructure; the inset at the bottom left corner is Fourier transformation of the STEM image, showing the CDW modulation point. (c) Temperature dependence of resistivity for $1T$-$TaSe_2$, showing clear phase transition at 470 K. Insets are electron diffraction of C phase and IC phase, respectively.

bunches which were textured and arranged in a decussate pattern on TEM copper grids, as shown in the inset of Fig. S1 of the Supplemental Material [33]. It has been demonstrated that this kind of MWCNT network can serve as a good thermal dissipation pathway during UTEM observations. The $1T$-$TaSe_2$ samples are ~50 nm thick and suitable for fs-laser excitation during ultrafast structural measurements with better stability. The ultrafast electron diffraction observations were performed under an acceleration voltage of 160 kV with a LaB_6 photocathode driven by 300 fs laser pulses (wavelength 347 nm, repetition rate 100 kHz). The photoinduced phase transition was initiated by another fs pump laser (wavelength 520 nm). We performed the experiments at 100 K, using an *in situ* low-temperature TEM holder for better, more stable results.

Three diffraction patterns obtained at different time delays with pump fluence (F) of 2 mJ/cm^2 are shown in Fig. 2(a). They are taken from a $1T$-$TaSe_2$ crystal oriented along the [001] zone axis direction. The satellite spots following the main diffraction spots can be used to characterize temporal evolution of the CDW transition in $1T$-$TaSe_2$. Considering the weak reflecting intensity of the satellite spots, we first collected the ultrafast data with the electron bunches containing ~1000 electrons/pulse, by integration of 10^5 electron pulses. The electron beam was converged to about 10 micrometers, and we selected an area of 5 micrometers for diffraction. One of the most notable features in these diffraction patterns is the change of intensity and position of the CDW satellite spots upon photoexcitation. As similarly discussed in UED studies [21,22], the intensity decrease of the satellite spots under low laser fluences in this kind of layered CDW system can be well explained by the atomic motions resulting from temporal evolution of the electronic spatial distribution and strong

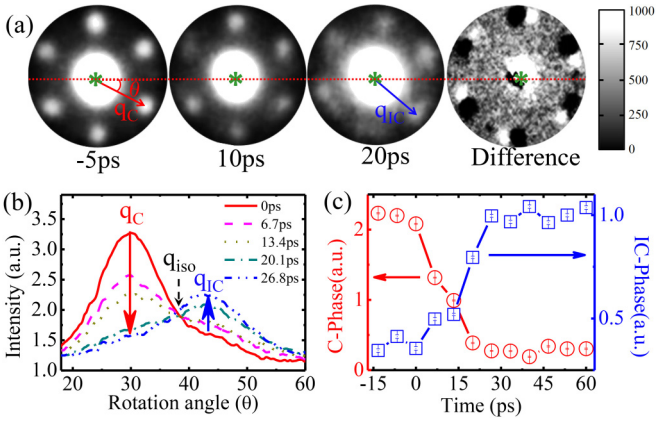

FIG. 2. (Color online) Time-resolved experimental data for CDW transition of $1T$-$TaSe_2$ with a fluence of 2.0 mJ/cm^2, showing the "structural isosbestic point" for the CDW transition. (a) Diffraction patterns for time delays of −5, 10, and 20 ps. Visible in the difference between −5 and 20 ps is the rotation of the satellite reflections. (Contrast of the difference was manually adjusted for clarity). (b) Angular integrated one-dimensional diffraction curves for different time delays. (c) Time dependence of the CDW intensity for C phase and IC phase.

electron-phonon coupling. In the present study, our UTEM investigations are focused mainly on the notable changes of CDW modulations associated with the phase transitions induced by laser excitation. To facilitate comparison, the diffraction difference between the two frames captured at −5 ps and 20 ps is also displayed in the right frame of Fig. 2(a), highlighting the visible rotation of the CDW modulation. The rotation angle (~13°) is fundamentally consistent with the data as thermally measured for the phase transition at $T_C = 470$ K. Very recently, this relevant CDW transition between commensurate and incommensurate state in $1T$-TaS_2 has been investigated by UED in Ref. [34].

For a better, clearer view of these CDW dynamic features, we theoretically analyzed all diffraction patterns using angular integration, yielding a one-dimensional curve in which the position shifts for CDW spots can be clearly exhibited. Actually, it is also convenient to characterize the phase transition in $1T$-$TaSe_2$ by using the modulation wave vector q, which changes in accord with the time delay and excitation fluence. Alterations of wave vector and spot intensity can be directly measured in comparison with the $t = 0$ frame as shown in Figs. 2(b) and 2(c). We first discuss the interconversion between the two CDW states, IC phase and C phase. In this CDW system, this nonequilibrium phase transition reveals a noteworthy "structural isosbestic point," clearly illustrated in Fig. 2(b). This reflects the characteristics of the microscopic process of ultrafast phase transition. A similar structural feature has been discussed in the literature for the $La_2CuO_{4+\delta}$ high-T_c superconductor, in which the "isosbestic point" for the alteration of interlayer space is interpreted by photodoping effects [35]. From a structural point of view, for this CDW transition, the existence of an isosbestic angle for the wave vector (q_{iso}) demonstrates that the IC phase and C phase yield their diffracting efficiencies in an equal ratio at this specific transient point [35,36]. Actually, we can described this phenomenon by a very general expression:

the electron diffraction amplitude is the Fourier transform of the lattice potential for the $q_{\rm iso}$ reciprocal vector, $A(q_{\rm iso}) = \Sigma_{H,j} V_H \exp[2\pi i(H - q_{\rm iso})r_j]$ (where the coefficient V_H is the lattice potential obtained from a Fourier transform of the reciprocal lattice vector H). So the diffraction intensity is essentially governed by alteration of the atomic position (r_j) in the transient state. Therefore, the presence of the "isosbestic point" demonstrates that the atomic structure in the crystal planes parallel to the vector $q_{\rm iso}$ reveals very similar dynamic features in the two phases, IC phase and C phase. Just as in a spectroscopy study in chemical kinetics [37], the "isosbestic point" corresponds to a wavelength at which the absorption spectra of two species coincide. The "structural isosbestic point" for the CDW transition implies that these two CDWs yield constant diffraction intensity throughout the whole photoinduced nonequilibrium transition. Moreover, the ultrafast change of the diffraction intensity of the satellite spots—in particular, the orientation of the isosbestic wave vector ($q_{\rm iso}$)—plays a critical role in explaining both the electron-phonon coupling and the atomic motion within related crystal planes. Based on experimental measurements, we can estimate $q_{\rm iso}$ using $q_{\rm iso} \approx (2q_C + 3q_{\rm IC})/5$, as shown in Fig. 2(b), so the $q_{\rm iso}$ vector could approximately align with the [120] zone axis direction and the crystallographically equivalent directions [38]. This fact suggests that the (120) crystal planes could be critical to an understanding of the transient states in the CDW interconversion through a nonequilibrium phase transition. The decay of the CDW state in the C phase and the formation of the incommensurate state in the IC phase have been analyzed and calculated based on the alteration of the diffraction intensity of satellite spots, as illustrated in Fig. 2(c), in which we have selected two Gaussian functions to fit the experimental data after the inelastic background is subtracted. As a result, the dynamic alternations of volume fraction for the C phase and the IC phase are clearly illustrated in a time scale of picoseconds.

Considering the presence of visible space-charge effects in the ultrafast imaging process, we improved the temporal resolution of the experimental data by lowering the probe laser power applied to obtain photoemission. As a result, each electron pulse contains about 10 electrons, and the pulse duration is estimated to be about 1 ps (FWHM) at the sample position, as reported in our previous publication [20]. We obtained a series of experimental diffraction patterns with $F = 1.8$ mJ/cm^2. Each pattern for this ultrafast process is taken with an exposure time of 30 seconds. Figure 3(a) (bottom panel) depicts observed trajectories in momentum-time space for two CDW modulations with a clear switch of wave vectors. This picture shows the temporal evolution of the CDW satellite spots in the q-t space as a three-dimensional plot, in which intensity at 30 degrees represents the diffraction signal for the C phase, and the signal at around 43 degrees represents the diffraction signal for the IC phase. In order to clearly illustrate the alteration of local atomic configurations, we also show the superstructure models for the C phase before time zero (t_0) (upper left panel) and the IC phase structure (upper right panel) with visible atomic shifts. Figure 3(b) shows experimental data for the intensity of satellite spots for the C phase and IC phase obtained from 0 to 20 ps, in which the experimental data have been fitted using a method similar to the one mentioned with

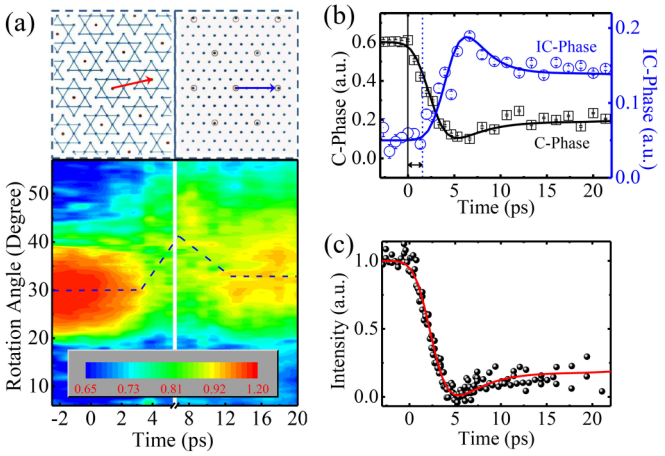

FIG. 3. (Color online) Dynamic features and temporal evolution of the CDW transition from C phase to IC phase. (a) Alteration of the CDW state at pump fluence of 1.8 mJ/cm^2. The CDW transition reveals a three-step transient feature: the CDW melting in the C phase, then the charge reordering in the IC phase, and then partial recovery from IC phase to C phase. The upper panels show two structural models illustrating the local atomic order in C phase and IC phase respectively. (b) The intensity changes of satellite spots for q_C and $q_{\rm IC}$ as a function of time delay. (c) Time dependence of C phase intensity, averaging five sets of experimental data, illustrating the CDW melting process. Experimental data for each sample have been normalized with the values of time zero (set as 1) and the minimum point at around 5 ps (set as 0).

regard to Fig. 2. In order to facilitate further analysis of the CDW melting nature in the C phase, we show in Fig. 3(c) the intensity of the satellite spots, averaged from five sets of experimental data.

Careful analysis of dynamic change of the CDW states suggests that the photoinduced phase transition in 1T-TaSe$_2$ contains three transient steps: C-phase suppression, IC-phase growth, and a partial CDW reordering from the IC to the C phase. According to our UTEM investigation and similar measurements performed in previous UED studies, the CDW melting in the C phase can be expressed as $I(t)/I_0 = C_1 \exp(-t/t_1) + C_2[1 - \exp(-t/t_2)]$, where the first term illustrates the CDW melting in the C phase and the second term represents the recovery of the C phase. According to previous UED data of similar CDW system [21–23], the melting of CDW happened in the 300–500 fs timescale. In our data fitting and analysis, the time constant (t_1) for C-phase suppression was set as 1 ps. Actually, we successfully fitted the experimental data using this expression convoluted with the instrument response function [39], as shown in Figs. 3(b) and 3(c). The recovery time constant is found to be 3±1 ps for the C phase, similar to that reported for 1T-TaS$_2$ [21]. Moreover, this CDW transition reveals certain notable nonconcerted features; e.g., the commensurate CDW melting and the incommensurate CDW reordering occur in different time scales. Figure 3(b) shows clearly that a time delay (about 2 ps) exists between the C-phase suppression and the IC-phase growth. In the present ultrafast photoinduced phase transition, first the hot electrons were generated by pumping laser, which directly induced CDW melting. Then, the energy was transferred from the electronic system to phonons at a characteristic time scale

of around 300–500 fs; then the state relaxes through further electron-phonon and phonon-phonon pathways which leads to lattice heating. The time delay as observed in our measurement manifests that the formation of IC phase is followed by the electron-phonon energy transfer. This suggests that the photoinduced CDW transition in $1T$-$TaSe_2$ is thermally driven, as has been discussed and debated in the literature [21,22]. The CDW recovery time (3 ± 1 ps) from IC phase to C phase is consistent with the results reported for $1T$-TaS_2 (4 ps) [21] and $1T$-$TiSe_2$ (1 ps) [40]. However, the $4H_b$-$TaSe_2$ phase is reported to show a much longer recovery time of about 150ps, which was attributed to effects of the three-dimensionality of the CDW, as discussed in Ref. [22]. It is believed that the CDW recovery dynamics in this time scale are dominated by the energy transport and conversion associated with acoustic phonon thermalization. This phenomenon is essentially correlated with anharmonic phonon decay, a relationship which is critical to an understanding of the coupled electron-lattice order parameters, as similarly discussed in Ref. [21].

Though measurements of physical properties at the CDW transitions in the $1T$-$TaSe_2$ crystals clearly show first-order characteristics with respect to thermal equilibrium [3,41,42], our UTEM study of the ultrafast structural changes of the order parameters reveals rather different characteristics in many cases. It is known that the photoinduced CDW transition is essentially a nonequilibrium phase transition. In order to qualitative illustrate transient states and better understand the photoinduced CDW transition, we herein just present a brief discussion of our data in comparison with the BCS approximation. The CDW intensity, in general, changes gradually through the phase transition, due to the appearance of transient states. Actually, modification of the CDW intensity is the main determinant of the thermodynamic properties of the phase transitions [43]. Indeed, a previous UED study showed that a photoinduced nonequilibrium phase transition in $4H_b$-$TaSe_2$ contains clear second-order characteristics [22]. Furthermore, the CDW transition can also be well addressed using atomic displacement amplitude as a function of the excitation density, and the CDW intensity can be written as $I_{\mathrm{CDW}} \propto (Q \cdot A)^2$, where Q is the CDW wave vector and A is the atomic displacement [22,43]. Figure 4(a) exhibits the change of atomic displacements (i.e., the order parameter) as a function of laser fluence, illustrating the complex nature of the CDW transition in $1T$-$TaSe_2$. We herein show a quantitative analysis using the BCS approximation, which is used fundamentally for study of the thermal equilibrium transition. It can be seen that the results obtained at the time delay of 20 ps can be well fitted by $I_{\mathrm{CDW}} = \tanh[1.78(F_c/F - 1)^{1/2}]$, i.e., the known BCS expression for the second-order phase transitions [44]. On the other hand, the relative atomic displacement changes measured at other time delays often appear at regions between the first- and second- order transitions; e.g., the experimental data obtained at $t = -20$ ps (blue dots). This feature is believed to arise from lattice thermalization, complex transient structures,

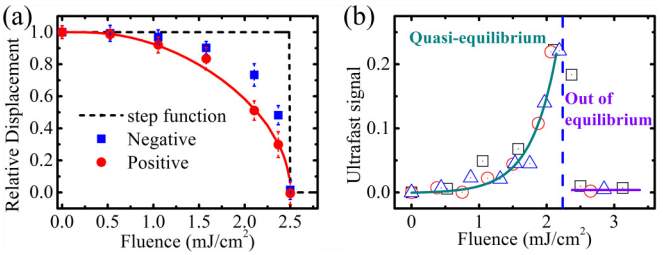

FIG. 4. (Color online) Fluence dependence of order parameter and transient diffraction signal. (a) Relative displacement as a function of laser fluence at a time delay of $t = 20$ ps (positive) and -20 ps (negative). The structural evolution at the time delay of 20 ps has been fitted by a BCS function. The structural evolution at the time delay of -20 ps appears at the region between the first- and second-order transitions. (b) The changes of ultrafast diffraction difference as a function of laser fluence. A nonlinearly increasing region and an irreversible region are indicated.

and structural alteration with a tendency of the first-order transitions. Note that, in general, the intensity of the CDW spots decreases nonlinearly with increasing laser fluence [see Fig. 4(b)]. Moreover, when the fluence exceeds 2.2 mJ/cm^2, defect structures and twinning can be commonly introduced in the samples, which could yield irreversible features in the UTEM experiments.

In summary, through photoexcitation, a CDW transition from the C phase to the IC phase was observed by UTEM investigations, and a rich variety of fast changes of CDW direction and intensity were clearly observed and identified in correlation with structural interconversion and charge reconfiguration. Moreover, the transition of superstructure reveals a notable "structural isosbestic point," resulting from the competition and/or coexistence of two CDW phases during this nonequilibrium phase transition. Certain fundamental features and second-order characteristics in the transient states were also analyzed for this photoinduced CDW transition. Our study demonstrates that with further UTEM improvements of spatial and/or temporal resolutions and an increase in the signal-to-noise ratio, the combination of real-space imaging and reciprocal space diffraction in 4D-UTEM will make it possible to explore the specific charge and atomic motions in strongly correlated systems.

This work was supported by the National Basic Research Program of China 973 Program (Grants No. 2011CBA00101, No. 2015CB921300, No. 2012CB821404, and No. 2011CBA00111), the Natural Science Foundation of China (Grants No. 91221102, No. 11190022, No. 11474323, No. 51272277, No. 11274368, No. 91422303, and No. U1232139), and the "Strategic Priority Research Program (B)" of the Chinese Academy of Sciences (Grants No. XDB07020300 and No. XDB07020200).

S.S.S. and L.L.W. contributed equally to this work.

[1] Y. Liu, R. Ang, W. J. Lu, W. H. Song, L. J. Li, and Y. P. Sun, Appl. Phys. Lett. **102**, 192602 (2013).

[2] R. Ang, Y. Miyata, E. Ieki, K. Nakayama, T. Sato, Y. Liu, W. J. Lu, Y. P. Sun, and T. Takahashi, Phys. Rev. B **88**, 115145 (2013).

[3] J. A. Wilson, F. J. Di Salvo, and S. Mahajan, Phys. Rev. Lett. **32**, 882 (1974).

[4] L. Pfeiffer, T. Kovacs, and F. J. Di Salvo, Phys. Rev. Lett. **52**, 687 (1984).

[5] H. Schäfer, V. V. Kabanov, M. Beyer, K. Biljakovic, and J. Demsar, Phys. Rev. Lett. **105**, 066402 (2010).

[6] F. Schmitt, P. S. Kirchmann, U. Bovensiepen, R. G. Moore, L. Rettig, M. Krenz, J.-H. Chu, N. Ru, L. Perfetti, D. H. Lu, M. Wolf, I. R. Fisher, and Z.-X. Shen, Science **321**, 1649 (2008).

[7] A. Tomeljak, H. Schäfer, D. Städter, M. Beyer, K. Biljakovic, and J. Demsar, Phys. Rev. Lett. **102**, 066404 (2009).

[8] T. Rohwer, S. Hellmann, M. Wiesenmayer, C. Sohrt, A. Stange, B. Slomski, A. Carr, Y. Liu, L. M. Avila, M. Kalläne, S. Mathias, L. Kipp, K. Rossnagel, and M. Bauer, Nature (London) **471**, 490 (2011).

[9] V. R. Morrison, R. P. Chatelain, K. L. Tiwari, A. Hendaoui, A. Bruhács, M. Chaker, and B. J. Siwick, Science **346**, 445 (2014).

[10] B. J. Siwick, J. R. Dwyer, R. E. Jordan, and R. J. D. Miller, Science **302**, 1382 (2003).

[11] M. Hada, K. Pichugin, and G. Sciainia, Eur. Phys. J. Spec. Top. **222**, 1093 (2013).

[12] M. Chergui and A. H. Zewail, Chem. Phys. Chem. **10**, 28 (2009).

[13] M. Bargheer, N. Zhavoronkov, M. Woerner, and T. Elsaesser, Chem. Phys. Chem. **7**, 783 (2006).

[14] A. Cavalleri, C. Tóth, C. W. Siders, J. A. Squier, F. Ráksi, P. Forget, and J. C. Kieffer, Phys. Rev. Lett. **87**, 237401 (2001).

[15] L. Piazza, D. J. Masiel, T. LaGrange, B. W. Reed, B. Barwick, and F. Carbone, Chem. Phys. **423**, 79 (2013).

[16] L. Piazza, T. T. A. Lummen, E. Quiñonez, Y. Murooka, B. W. Reed, B. Barwick, and F. Carbone, Nat. Commun. **6**, 6407 (2015).

[17] B. Barwick, H. S. Park, O. H. Kwon, J. S. Baskin, and A. H. Zewail, Science **322**, 1227 (2008).

[18] B. W. Reed, T. LaGrange, R. M. Shuttlesworth, D. J. Gibson, G. H. Campbell, and N. D. Browning, Rev. Sci. Instrum. **81**, 053706 (2010).

[19] L. Piazza, C. Ma, H. X. Yang, A. Mann, Y. Zhu, J. Q. Li, and F. Carbone, Struct. Dyn. **1**, 014501 (2014).

[20] G. L. Cao, S. S. Sun, Z. W. Li, H. F. Tian, H. X. Yang, and J. Q. Li, Sci. Rep. **5**, 8404 (2015).

[21] M. Eichberger, H. Schäfer, M. Krumova, M. Beyer, J. Demsar, H. Berger, G. Moriena, G. Sciaini, and R. J. D. Miller, Nature (London) **468**, 799 (2010).

[22] N. Erasmus, M. Eichberger, K. Haupt, I. Boshoff, G. Kassier, R. Birmurske, H. Berger, J. Demsar, and H. Schwoerer, Phys. Rev. Lett. **109**, 167402 (2012).

[23] P. Zhu, J. Cao, Y. Zhu, J. Geck, Y. Hidaka, S. Pjerov, T. Ritschel, H. Berger, Y. Shen, R. Tobey, J. P. Hill, and X. J. Wang, Appl. Phys. Lett. **103**, 071914 (2013).

[24] L. Stojchevska, I. Vaskivskyi, T. Mertelj, P. Kusar, D. Svetin, S. Brazovskii, and D. Mihailovic, Science **344**, 177 (2014).

[25] Y. Ge and A. Y. Liu, Phys. Rev. B **82**, 155133 (2010).

[26] K. Horiba, K. Ono, J. H. Oh, T. Kihara, S. Nakazono, M. Oshima, O. Shiino, H. W. Yeom, A. Kakizaki, and Y. Aiura, Phys. Rev. B **66**, 073106 (2002).

[27] L. Perfetti, A. Georges, S. Florens, S. Biermann, S. Mitrovic, H. Berger, Y. Tomm, H. Hochst, and M. Grioni, Phys. Rev. Lett. **90**, 166401 (2003).

[28] S. Colonna, F. Ronci, A. Cricenti, L. Perfetti, H. Berger, and M. Grioni, Phys. Rev. Lett. **94**, 036405 (2005).

[29] F. Clerc, C. Battaglia, H. Cercellier, C. Monney, H. Berger, L. Despont, M. G. Garnier, and P. Aebi, J. Phys.: Condens. Matter **19**, 355002 (2007).

[30] M. Eibschutz, Phys. Rev. B **45**, 10914 (1992).

[31] R. Brouwer and F. Jellinek, Physica B&C **99**, 51 (1980).

[32] B. Giambattista, C. G. Slough, W. W. McNairy, and R. V. Coleman, Phys. Rev. B **41**, 10082 (1990).

[33] See Supplemental Material at http://link.aps.org/supplemental/10.1103/PhysRevB.92.224303 for further details of the experiment technique and the fitting procedure.

[34] T.-R. T. Han, F. Zhou, C. D. Malliakas, P. M. Duxbury, S. D. Mahanti, M. G. Kanatzidis, and C.-Y. Ruan, Sci. Adv. **1**, e1400173 (2015).

[35] N. Gedik, D. Yang, G. Logvenov, I. Bozovic, and A. H. Zewail, Science **316**, 425 (2007).

[36] D.-S. Yang and A. H. Zewail, Proc. Natl. Acad. Sci. USA **106**, 4122 (2009).

[37] R. G. Mayer and R. S. Drago, Inorg. Chem. **15**, 2010 (1976).

[38] Based on experimental measurements, $q_C = 0.225a^* + 0.07b^*$; actually, $q_{IC} = 0.278a^*$ has other crystallographically equivalent directions, such as $0.278a^*$, $0.278(a^* - b^*)$, and $0.278b^*$. If we use $q_{IC} = 0.278b^*$ and $q_{iso} \approx (2q_C + 3q_{IC})/5$, we can get the q_{iso} vector approximately aligned with the [120] zone axis.

[39] The instrument response function is a Gaussian function with a FWHM of 1 ps.

[40] E. Möhr-Vorobeva, S. L. Johnson, P. Beaud, U. Staub, R. De Souza, C. Milne, G. Ingold, J. Demsar, H. Schaefer, and A. Titov, Phys. Rev. Lett. **107**, 036403 (2011).

[41] A. Suzuki, T. Yamashita, K. Matsui, and M. Doyama, J. Phys. Soc. Jpn. **57**, 1707 (1988).

[42] K. Nakanishi and H. Shiba, J. Phys. Soc. Jpn. **43**, 1839 (1977).

[43] W. L. McMillan, Phys. Rev. B **12**, 1187 (1975).

[44] R. Meservey and B. Schwartz, in *Superconductivity*, edited by R. Park (Marcel Dekker, New York, 1969), Vol. 1, p. 117.